THE JOURNAL OF PHYSICAL CHEMISTRY C
A JOURNAL OF THE AMERICAN CHEMICAL SOCIETY

pubs.acs.org/JPCC

Article

Bimetallic FeO_x–MO_x Loaded TiO_2 (M = Cu, Co) Nanocomposite Photocatalysts for Complete Mineralization of Herbicides

Published as part of The Journal of Physical Chemistry virtual special issue "Michael R. Hoffmann Festschrift".

Ayoola Shoneye, Haimiao Jiao, and Junwang Tang*

Cite This: https://doi.org/10.1021/acs.jpcc.2c06796

Read Online

ACCESS | Metrics & More | Article Recommendations | Supporting Information

ABSTRACT: A series of monometallic and bimetallic cocatalyst(s), comprising FeO_x, CuO_x, CoO_x, FeO_x–CuO_x, and FeO_x–CoO_x loaded TiO_2 catalysts prepared by the surface impregnation method, were investigated for the photocatalytic mineralization of the widely used four herbicides: 2,4-dichlorophenol (2,4-DCP), 2,4,6-trichlorophenol (2,4,6-TCP), 2,4-dichlorophenoxyacetic acid (2,4-D), and 2,4,5-trichlorophenoxyacetic acid (2,4,5-T). It was found that FeO_x–CoO_x/TiO_2 showed the highest photocatalytic efficiency toward mineralization of selected herbicides. FeO_x–CoO_x/TiO_2 achieves 92% TOC removal in 180 min, representing nearly three time activity of the benchmark PC50 TiO_2. From XPS analysis, FeOOH, CuO, and CoO were determined to be loaded onto the TiO_2 surface. The outstanding photocatalytic performance of the optimized FeO_x–CoO_x/TiO_2 sample for herbicides mineralization is due to an increased charge separation and enhanced hydroxyl radicals production monitored by diverse spectroscopies. Based on the proposed charge transfer mechanism, FeO_x–CoO_x cocatalyst species accelerate the transfer of photogenerated holes on TiO_2, thus facilitating hydroxyl radicals production.

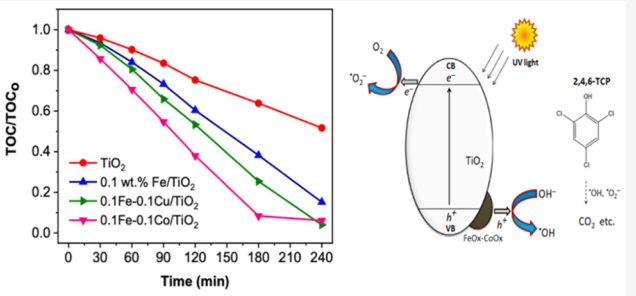

1. INTRODUCTION

Water pollution by toxic and persistent pollutants is a growing concern globally due to the increase in world population and the corresponding high demand for clean water for domestic and commercial use. It was reported that over 3.3 billion people (representing over 40% of the world population) lack access to clean water or live in water-stressed areas.[1−3] Chlorophenols and chlorinated herbicides are major sources of pollution among various organic water contaminants.[4] These pollutants are released into the environment (surface and underground waters) due to agricultural, nonagricultural, and industrial activities.[4,5] Most of these environmental persistent chlorinated herbicides are considered toxic or potentially carcinogenic to human and aquatic life and are listed among priority pollutants by US EPA.[6]

Advanced oxidation processes, such as TiO_2 photocatalysis, is gaining considerable attention as a reliable alternative to conventional water treatment technologies, for the safe destruction of persistent organic water pollutants.[7−9] TiO_2 is the most reported material for photocatalytic degradation of organic water pollutants. This is due to its low cost, high stability, and low toxicity to human and aquatic lives.[9−11] Apart from poor visible light activity, one of the major challenges with TiO_2 photocatalysis is the low charge separation efficiency of photogenerated electrons and holes, which dominates the overall photocatalytic efficiency for the degradation of targeted organic pollutants.

Surface modification of TiO_2 with earth-abundant cocatalysts, such as iron, copper, and cobalt oxides, to enhance photocatalytic degradation of chlorinated herbicides, has been widely reported in the literature.[12−14] Unlike the widely reported codoping of TiO_2 with Fe and/or Cu as dopants,[15−17] the use of binary cocatalysts on surface modification of TiO_2 for photocatalytic water treatment was relatively less reported. A binary codeposition of Ag and Cu nanoparticles on TiO_2, prepared via photodeposition, was reported for photocatalytic degradation of methylene blue dye and salicylic acid under UV and visible light irradiation.[18] The Ag–Cu–TiO_2 sample showed higher degradation efficiency compared to the monometallic (Ag or Cu) deposited TiO_2. The observed enhancement in photocatalytic activity was reported to be due to extended optical absorption, as a result of surface plasmonic effect. In addition, charge separation is more efficient compared to monometallic (Ag/Cu)–TiO_2 samples, as revealed by photoluminescence spectra measurements. A bi-co-catalyst alloy involving CuO and CoO (1 wt % Cu and 1 wt

Received: September 24, 2022
Revised: December 1, 2022

% Co) has been reported to improve the hydrogen evolution rate of SnO_2@TiO_2 in photocatalytic water splitting under UV light irradiation.[19] Also, CuO exhibited higher activity than CoO regarding single cocatalyst-decorated samples. The enhancement in H_2 evolution rate by CuO−CoO/SnO_2@TiO_2 was attributed to the synergistic improvement in the transfer of photogenerated electrons by CuO for reduction reaction and holes by CoO for oxidation reaction on the catalyst's surface. In another study involving single cocatalysts comparison, CuO_x was reported to display higher activity compared to FeO_x for the photocatalytic degradation of 4-chlorophenol (4-CP) in aqueous solution with TiO_2 under UV light irradiation.[20] Accordingly, constructing bimetallic TiO_2 based photocatalysts provides a very promising strategy to improve the photocatalytic efficiency in the field of photocatalytic degradation of chlorinated herbicides, benefiting from the desired advantages of bimetallic species such as their synergetic effects and electronic interactions within dual metal species.[21] Moreover, the development of efficient non-noble bimetallic cocatalysts is also preferable, which could greatly reduce the cost of photocatalysts. In one of our recent reports, FeOOH loaded TiO_2 exhibited superior performance in photocatalytic herbicides mineralization.[12] Thus, the combination of Fe and other low cost metal species such as Co and Cu as bimetallic cocatalysts to further enhance the efficiency of photocatalytic mineralization of herbicides is scarcely reported and is worthy to be thoroughly studied.

Herein, novel nanoarchitecture comprising binary metal oxides/hydroxides as cocatalysts on PC50 (commercial benchmark anatase TiO_2), were synthesized using a reproducible surface impregnation method. The Fe(III), Cu(II), and Co(II) species were characterized in order to clarify their functionality and actual active species. The photocatalytic degradation of 2,4,6-TCP and 2,4-D in water were carried out under UV/vis light irradiation. The effects of single cocatalysts, the dual cocatalyst coupling containing FeOOH as reported earlier,[12] the nature of the herbicide, and the light wavelength were investigated. Photocatalytic mineralization ability of the optimized catalyst was also evaluated with other widely used herbicides, 2,4-DCP and 2,4,5-T, to demonstrate its wide applications. The charge transfer mechanism was also discussed.

2. EXPERIMENTAL SECTION

2.1. Chemicals. PC50 TiO_2 (purely anatase) was purchased from Millennium Chemicals. 2,4,6-Trichlorophenol (98%) was purchased from Alfa Aesar. 2,4-Dichlorophenoxyacetic acid was purchased from Cayman Chemical Company. 2,4-Dichlorophenol (99%) and coumarin were purchased from Acros Organics. 2,4,5-Trichlorophenoxyacetic acid, Fe$(NO_3)_3$.$9H_2O$, Cu$(NO_3)_2$·$2.5H_2O$, and Co$(NO_3)_2$·$6H_2O$ were purchased from Sigma-Aldrich. 2-Propanol (HPLC grade) and acetonitrile (HPLC grade) were purchased from Fisher Scientific. All reagents were used as received without further purification.

2.2. Sample Preparation. A modified surface impregnation and drying technique was used to prepare dual cocatalyst-decorated TiO_2 composites.[12,22] In a typical experiment, the appropriate percentage weight of the nitrate precursors of Fe(III), Cu(II), and Co(II) was separately added to an aqueous suspension of 1.0 g of commercial PC50 TiO_2 under mild stirring, with M/TiO_2 composition (M is the metal with a weight percentage of 0.05, 0.1 and 0.5). The obtained slurry was continuously stirred with a magnetic stirrer bar and dried slowly at 80 °C on a hot plate. The resultant dried powder was hand-milled and calcined in a muffle furnace under air atmosphere at 250 °C for 4 h. It was collected after cooling to room temperature, washed, dried and hand-milled again, and stored for photocatalytic activity tests and characterizations. Subsequent studies on cocatalyst coupling (FeO_x−CuO_x/TiO_2 and FeO_x−CoO_x/TiO_2) were evaluated using optimum cocatalyst loading (0.1 wt % for each of the three cocatalysts), followed by a study on the photocatalytic performance of optimized photocatalyst for the mineralization of the four herbicides (2,4-DCP, 2,4,6-TCP, 2,4-D, and 2,4,5-T) under similar operating conditions.

2.3. Characterization of Photocatalysts. X-ray photoelectron spectroscopy (XPS) was performed by a Thermo Scientific K-alpha/NEXSA photoelectron spectrometer using monochromatic Al Kα radiation (1486.6 eV); peak positions were calibrated to carbon (284.5 eV) and plotted using the CasaXPS software. UV−vis absorption spectra measurements of powdered samples were performed using a Shimadzu UV-2550 spectrophotometer fitted with an integrating sphere. Inductively coupled plasma atomic emission spectroscopy (ICP-AES) was performed using Varian 720 to investigate the metal leaching. Hydroxyl radicals generated were quantified using aqueous coumarin solution and a Shimadzu RF-6000 Spectrofluorometer.

2.4. Photocatalytic Measurements. A 300 W Xe lamp (Newport) was used as the light source with a plain glass window (λ > 320 nm) as a cutoff filter. The glass window shields all UV light with wavelength <320 nm. In a typical measurement, 0.1 g of photocatalyst was dispersed in 200 mL of herbicide solution prepared with deionized water. The suspension was sonicated in an ultrasonic water-bath for 15 min and then magnetically stirred in the dark for 1 h to achieve adsorption/desorption equilibrium of herbicides on the photocatalyst. Thereafter, the suspension was irradiated with UV/visible light under continuous magnetic stirring, while the reaction vessel was immersed in a water-bath to regulate temperature ($T \leq 30$ °C). Upon light irradiation, a 3 mL sample portion was taken at regular time intervals and filtered through a micropore syringe filter (PTFE, 0.2 μm) before further analysis. Further studies with the best cocatalyst-decorated TiO_2 sample were carried out using 25 ppm 200 mL solution of four (4) different herbicides: 2,4,6-trichlorophenol (2,4,6-TCP), 2,4-dichlorophenol (2,4-DCP), 2,4-dichlorophenoxyacetic acid (2,4-D), and 2,4,5-trichlorophenoxyacetic acid (2,4,5-T).

2.5. Analyses. The change in herbicide concentration was measured using a high performance liquid chromatograph (HPLC-2030C, Shimadzu) consisting of a binary pump, an autosampler, a photodiode array detector and an ACE-5 C18 (5 μm × 150 mm × 4.6 mm) reverse phase column maintained at 40 °C. The HPLC used a 5−95% gradient (acetonitrile/H_2O with 0.1% formic acid) as the mobile phase.[12] A UV−vis spectrophotometer was also used to monitor herbicides degradation over the optimized sample. The further herbicides mineralization by photocatalysis was investigated primarily using a Shimadzu total organic carbon (TOC-L) analyzer.

3. RESULTS AND DISCUSSION

3.1. Characterization of FeO_x−MO_x/TiO_2 Nanocomposites. The absorption spectra of PC50 TiO_2 and the cocatalyst-decorated TiO_2 nanocomposites are shown in

https://doi.org/10.1021/acs.jpcc.2c06796
J. Phys. Chem. C XXXX, XXX, XXX−XXX

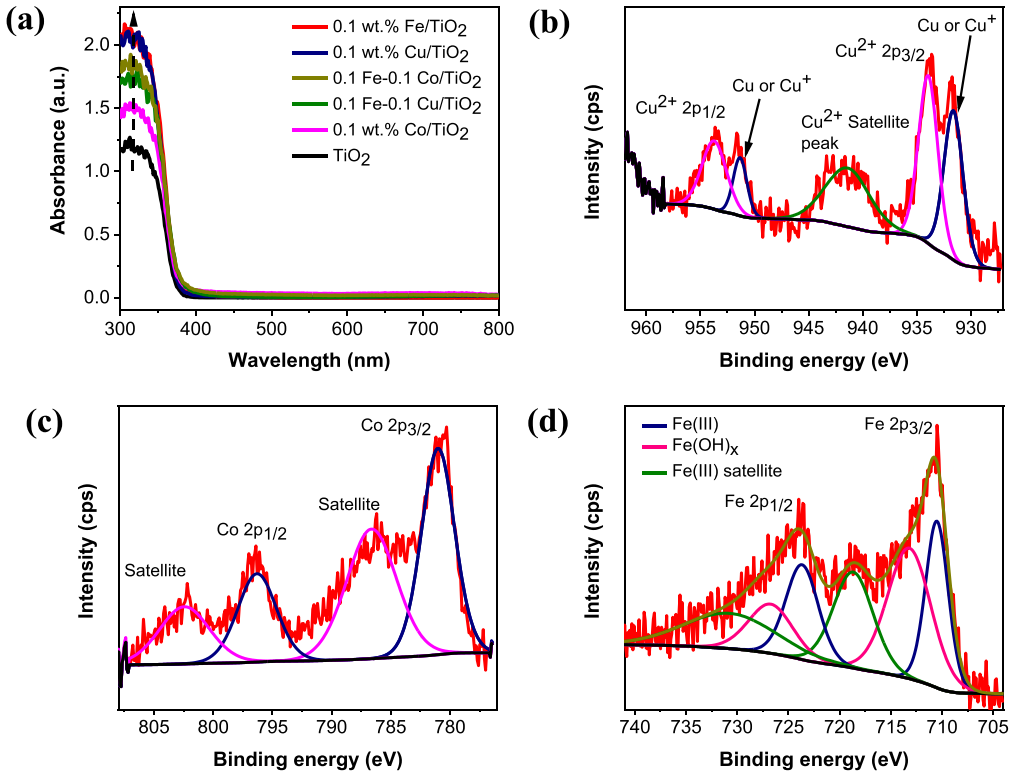

Figure 1. (a) UV/vis absorption spectra of prepared cocatalyst-decorated PC50 TiO_2 catalysts, (b) Cu 2p XPS spectra of FeO_x−CuO_x/TiO_2 sample with optimum Cu loading (0.1 wt % Cu and 0.1 wt % Fe), (c) Co 2p XPS spectra of FeO_x−CoO_x/TiO_2 sample with high Co loading (0.5 wt % Co and 0.5 wt % Fe), and (d) Fe 2p XPS spectra of FeO_x−CoO_x/TiO_2 sample with high Fe loading (0.5 wt % Fe and 0.5 wt % Co).

Figure 1a. Since the PC50 TiO_2 is white in color, it does not show any absorption in the visible region with a band gap of 3.2 eV. On the other hand, when dramatically increasing the cocatalyst loading amount, the photocatalysts represent somewhat color. For example, iron oxide-modified PC50 TiO_2 samples have light-yellow color that indicates the presence of Fe(III) oxide species,[22,23] which becomes reddish-brown with increase in FeO_x loading. The cobalt oxide modified PC50 TiO_2 samples have olive-green or gray color that indicates the presence of CoO,[13] which also becomes darker with increase in CoO loading. The copper oxide modified PC50 TiO_2 samples have light blue-green color, indicating the presence of CuO,[24] which also becomes gray and finally black with increase in CuO loading.

The XPS was used to identify the Fe, Cu and Co oxide species present in the FeO_x−CuO_x/TiO_2 and FeO_x−CoO_x/TiO_2 samples. Fe 2p, Cu 2p, and Co 2p peaks are very small observed in the full XPS survey spectrum of both samples (Figure S1), which is likely due to the low amount of cocatalysts loading and high dispersion on TiO_2 surface.[13,20] From the fitting Cu 2p XPS spectrum of FeO_x−CuO_x/TiO_2 in Figure 1b, peaks corresponding to Cu^{2+} are confirmed at 934 eV (Cu $2p_{3/2}$) and 954 eV (Cu $2p_{1/2}$).[25,26] A satellite peak characteristic of the presence of Cu^{2+} is clearly observed between 939−945 eV.[25] Apart from the Cu^{2+} satellite, the peak at binding energy of 931.6 eV is assigned to Cu/Cu^{+}.[14,26] However, it is difficult to differentiate between Cu_2O and Cu metal from the Cu 2p XPS peaks as their binding energies are too close and it is also difficult to identify them by other techniques due to very low amount loaded.[14,27] The Co 2p XPS spectrum of FeO_x−CoO_x/TiO_2 is of weak intensity due to low Co concentration in the sample as shown in Figure S2. Based on the fitting Co 2p XPS spectrum of FeO_x−CoO_x/TiO_2 (with high Co loading, 0.5 wt %) in Figure 1c, peaks corresponding to Co^{2+} are confirmed at 781 eV (Co $2p_{3/2}$) and 796 eV (Co $2p_{1/2}$).[26,28] The shakeup satellite features of Co^{2+} at 787 and 802 eV are very strong in intensity, which rules out the presence of Co^{3+}, whose satellite features are very weak in intensity at similar binding energies.[29,30] Also, the Fe 2p core-level XPS spectrum of FeO_x−CoO_x/TiO_2 is of weak intensity due to low Fe concentration in the sample as shown in Figure S3. Based on the fitting Fe 2p XPS spectrum of FeO_x−CoO_x/TiO_2 (with high Fe loading, 0.5 wt %) in Figure 1d, peaks corresponding to Fe^{3+} are confirmed at 710 eV (Fe $2p_{3/2}$) and 724 eV (Fe $2p_{1/2}$).[26,31−33] The satellite peaks at 719 and 733 eV are associated with the fingerprint of Fe(III) oxidation state.[32,33] The extra peaks at 713 and 728 eV are related to the influence of hydroxide groups.[32,33] Absence of a peak at 709 eV rules out the presence of Fe^{2+} in the sample.[31,34] Based on the Ti 2p core-level XPS spectra of TiO_2, FeO_x/TiO_2, FeO_x−CuO_x/TiO_2, and FeO_x−CoO_x/TiO_2 in Figure S4, peaks corresponding to Ti^{4+} are confirmed around 458 eV (Ti $2p_{3/2}$) and 464 eV (Ti $2p_{1/2}$).[25,31] A slight peak shift to lower energy is observed with FeO_x/TiO_2, while a slight shift to higher energy is observed with FeO_x−CuO_x/TiO_2 and FeO_x−CoO_x/TiO_2 compared to pristine TiO_2. The observation suggests that there is a form of strong interaction between TiO_2 and the dual cocatalysts, which is neither Ti^{4+} reduction nor oxidation.[32]

3.2. Photocatalytic Mineralization of Herbicides. First, the control experiment was carried out with only 2,4,6-TCP solution in the absence of a photocatalyst. Virtually 0% TOC removal is observed after 3 h of light irradiation as shown in Figure 2a. Photocatalytic activities of the as-prepared mono

https://doi.org/10.1021/acs.jpcc.2c06796
J. Phys. Chem. C XXXX, XXX, XXX−XXX

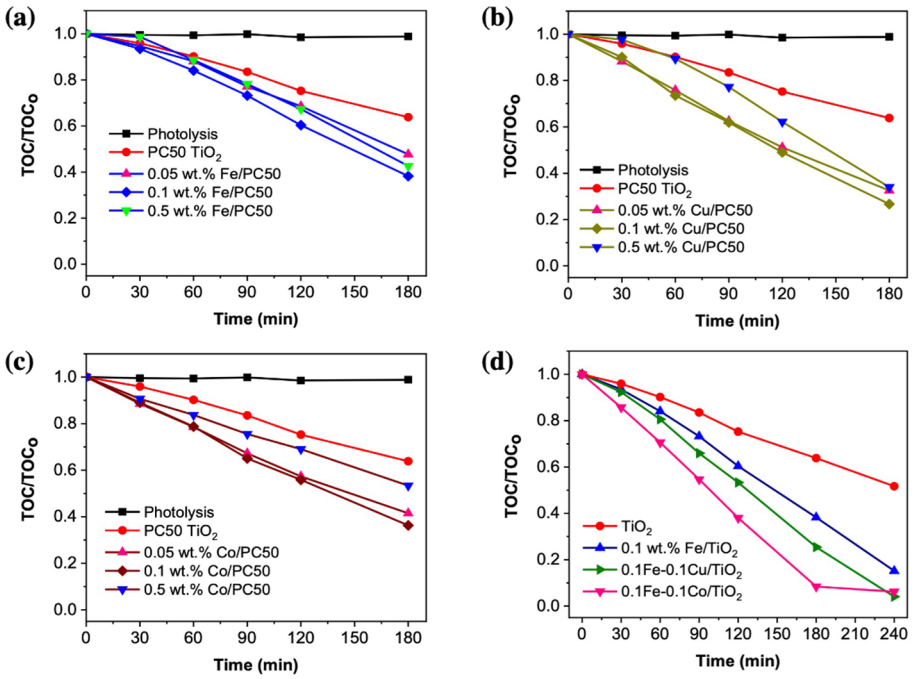

Figure 2. (a) Mineralization profiles of 2,4,6-TCP using FeO_x/TiO_2 with different Fe loading and control experiments, (b) mineralization profiles of 2,4,6-TCP using CuO_x/TiO_2 with different Cu loading and control experiments, (c) mineralization profiles of 2,4,6-TCP using CoO_x/TiO_2 with different Co loading and control experiments, (d) mineralization profiles of 2,4,6-TCP when using FeO_x as the primary cocatalyst and CuO_x or CoO_x as a second cocatalyst. The mineralization profiles were monitored by a TOC analyzer. Conditions: 2,4,6-TCP, 50 ppm, 200 mL, pH = 6, catalyst concentration = 0.5 g/L, and $\lambda > 320$ nm.

and dual cocatalyst-decorated TiO_2 composites were then evaluated by the mineralization of 2,4,6-TCP under full arc light irradiation ($\lambda > 320$ nm).

The 2,4,6-TCP mineralization rate recorded on PC50 TiO_2 is nearly 35% after 3 h. Approximately 52% TOC removal is achieved with the optimized 0.05 wt % Fe/TiO_2 sample after 3 h. An increase in Fe concentration up to 0.1 wt % leads to a further increase in photocatalytic activity, while lower 2,4,6-TCP mineralization rate is observed with 0.5 wt % Fe-loaded sample. The optimum condition for the preparation of FeO_x/TiO_2 nanocomposites is found to be 0.1 wt % Fe with ca. 62% TOC removal after 3 h. Similar trends were observed for Co and Cu concentrations as shown in Figures 2b and 2c. The optimum condition for the preparation of CuO_x/TiO_2 and CoO_x/TiO_2 nanocomposites are found also to be 0.1 wt % Cu and 0.1 wt % Co, with about 73% and 64% TOC removal after 3 h, respectively. An increase in the amount of cocatalyst (0.5 wt %) beyond the optimum negatively affects the photocatalytic activity.

This observation could be due to shielding of intrinsic light absorption by colorful cocatalysts and occupying the oxidation sites on TiO_2.[22] For the mono cocatalyst-loaded TiO_2 samples, the order of photocatalyst activity is $CuO_x > CoO_x \approx FeO_x$.

Next, the effect of dual cocatalyst loading, e.g., FeO_x–CuO_x and FeO_x–CoO_x was investigated based on optimum loading amount for individual cocatalyst (0.1 wt %). A graphical summary showing the influence of CuO_x on pristine TiO_2 and FeO_x/TiO_2 is displayed in Figure S5. The presence of CuO_x enhances the photocatalytic activity of both samples. About 73% and 75% TOC removal in 3 h are recorded with CuO_x/TiO_2 and FeO_x–CuO_x/TiO_2 samples, respectively for 2,4,6-TCP decomposition. A graphical summary showing the influence of CoO_x on pristine TiO_2 and FeO_x/TiO_2 is displayed in Figure S6. CoO_x also enhances the photocatalytic activity of both samples as observed with CuO_x. However, there is a remarkable enhancement in 2,4,6-TCP mineralization efficiency with the FeO_x–CoO_x/TiO_2 sample as it records about 92% TOC removal in 3 h. The influence of CuO_x and CoO_x on FeO_x/TiO_2 is clearly compared in Figure 2d. The photocatalytic 2,4,6-TCP mineralization efficiencies in 3 h follow the order: TiO_2 (36%) < FeO_x/TiO_2 (62%) < FeO_x–CuO_x/TiO_2 (75%) < FeO_x–CoO_x/TiO_2 (92%).

The 2,4,6-TCP degradation rates over TiO_2, FeO_x/TiO_2, FeO_x–CuO_x/TiO_2, and FeO_x–CoO_x/TiO_2 from HPLC measurements are compared in Figure 3. The 2,4,6-TCP degradation rates well agree with the 2,4,6-TCP mineralization rates, with the exception of FeO_x–CuO_x/TiO_2, as it performed less than FeO_x/TiO_2 in the first 90 min. The photocatalytic 2,4,6-TCP degradation efficiencies in 180 min follow the

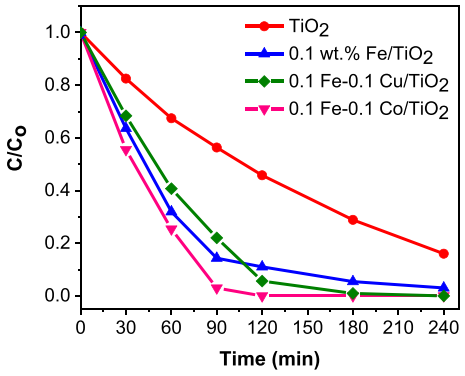

Figure 3. Conversion profiles of 2,4,6-TCP using TiO_2, FeO_x/TiO_2, FeO_x–CuO_x/TiO_2, and FeO_x–CoO_x/TiO_2 samples monitored by HPLC. Conditions: 2,4,6-TCP, 50 ppm, 200 mL, pH = 6, catalyst concentration = 0.5 g/L, $\lambda > 320$ nm.

https://doi.org/10.1021/acs.jpcc.2c06796
J. Phys. Chem. C XXXX, XXX, XXX–XXX

order: TiO_2 (71%) < FeO_x/TiO_2 (95%) < $FeO_x–CuO_x/TiO_2$ (99%) < $FeO_x–CoO_x/TiO_2$ (100%). Based on above results from HPLC and TOC measurements, $FeO_x–CoO_x/TiO_2$ shows comparable efficiency in both photocatalytic 2,4,6-TCP degradation (100%) and mineralization process (92%) in 180 min. Besides, it can see that the degradation rates of 2,4,6-TCP over different photocatalysts decrease continuously in the first 120 min, possibly due to the continuous decreasing pollutant concentration.[35] In contrast, the mineralization rates by TOC analysis over various samples gradually increases as the reaction progress at the same reaction time. Nevertheless, the 2,4,6-TCP degradation process (monitored by HPLC) is much faster over FeO_x, $FeO_x–CuO_x$, and $FeO_x–CoO_x$–decorated TiO_2 samples than its mineralization. It is because that it starts with fast partial oxidation of the benzene ring to form other organic products as intermediates, while the mineralization process is slow as the final step, which involves the complete breaking of the benzene ring to liberate carbon dioxide (CO_2).[36−38] An increase in the photocatalytic activities of the bi-co-catalysts-decorated TiO_2 samples compared to FeO_x-decorated TiO_2, is likely due to some synergistic effect from the cocatalyst alloys, which favors efficient separation of photogenerated electrons and holes during photocatalytic degradation of 2,4,6-TCP.

Fe(III) oxide species (mainly FeOOH as proved in our previous study[12]) have been reported to favor the improved generation of hydroxyl radicals as a hole acceptor in the literature.[12,39,40] It has been reported that Cu(II) oxide species facilitate the transfer of photogenerated electrons on surface of TiO_2 by enhancing oxygen reduction to generate superoxide radicals.[20,25] CoO_x has been reported to be a very good oxidation cocatalyst in photo-oxidation of organic compounds[41,42] and oxygen evolution in photocatalytic water splitting by improving the lifetime of photogenerated holes.[43−45]

The significant improvement in 2,4,6-TCP mineralization efficiency by $FeO_x–CoO_x$ compared to $FeO_x–CuO_x$ as bi-co-catalysts, as shown in Figure 2d, which is likely due to a high synergistic effect between FeO_x and CoO_x as good oxidation cocatalysts, thus resulting in improved electron/hole charge separation and generation of hydroxyl radicals for 2,4,6-TCP mineralization. The experimental error bar plot of the optimized $FeO_x–CoO_x/TiO_2$ is shown in Figure S7 after carrying out the 2,4,6-TCP mineralization experiment in triplicates. The result signifies that the experiment is repeatable to a large extent. The photocatalytic activity of the optimized $FeO_x–CoO_x/TiO_2$ sample was further evaluated under different light wavelengths and results are displayed in Figure 4. Virtually 0% TOC removal was observed after 3 h of light irradiation with a 395 nm cutoff filter. The outcome was not surprising, since surface impregnation of TiO_2 with cocatalysts does not change the band gap energy of the PC50 TiO_2 (ca. 3.2 eV) as represented in Figure 1a, which corresponds to light wavelength of around 390 nm. This further implies that the pristine and low concentration metal oxides-modified TiO_2 samples cannot absorb light of wavelength above 390 nm, which results into negligible 2,4,6-TCP degradation activity. However, with light irradiation of wavelength (λ > 260 nm), there is a remarkable enhancement in the 2,4,6-TCP mineralization rate in the first 2 h, compared to that of light irradiation of wavelength (λ > 320 nm). This is due to the availability of stronger UV light (UV−B) irradiation and contributions from 2,4,6-TCP photodegradation, since 2,4,6-TCP absorbs UV light below 320 nm.[12] Around 62% TOC removal was achieved with λ > 320 nm, while about 93% TOC removal was achieved with λ > 260 nm in 2 h.

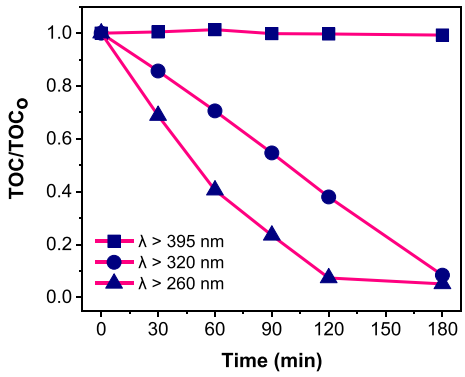

Figure 4. Mineralization profiles of 2,4,6-TCP using $FeO_x–CoO_x/TiO_2$ sample under different light wavelength (λ) ranges. Conditions: 2,4,6-TCP, 50 ppm, 200 mL, pH = 6, catalyst concentration = 0.5 g/L.

Further studies on photocatalytic mineralization ability of the optimized $FeO_x–CoO_x/TiO_2$ sample was evaluated with another widely used herbicide, 2,4-dichlorophenoxyacetic acid (2,4-D) and results are displayed in Figure 5a. Here, 0% TOC removal was observed after 3 h of light irradiation in the absence of a photocatalyst. Nearly 60%, 95%, and 100% TOC removal are achieved with the unmodified TiO_2, FeO_x/TiO_2, and $FeO_x–CoO_x/TiO_2$ samples in 3 h, respectively. 2,4-D removal by the optimized $FeO_x–CoO_x/TiO_2$ was also analyzed with HPLC, and results are shown in Figure 5b. The 2,4-D degradation rates well agree with the corresponding mineralization rates in the first 60 min. The photocatalytic 2,4-D degradation efficiencies in 60 min follow the order: TiO_2 (85%) < FeO_x/TiO_2 (91%) < $FeO_x–CoO_x/TiO_2$ (95%). Beyond 60 min, the three samples recorded approximately similar photocatalytic activity for 2,4-D degradation. This is likely due to the presence of very low concentration of 2,4-D in solution and on surface of the photocatalyst. Also, the 2,4-D degradation process is very fast over FeO_x and $FeO_x–CoO_x$-decorated TiO_2 samples compared to the slow mineralization process, since partial oxidation precedes the cleavage of the aromatic benzene ring to liberate carbon dioxide (CO_2).[36−38] The $FeO_x–CoO_x/TiO_2$ sample also shows the highest 2,4-D mineralization efficiency but similar 2,4-D degradation performance compared to FeO_x/TiO_2 and TiO_2. The experimental error bar plot of optimized $FeO_x–CoO_x/TiO_2$ is also shown in Figure S8 after carrying out the 2,4-D mineralization experiment in triplicates. The result shows that the experiment is highly reproducible.

In order to investigate how the chlorine substituents and other functional groups on the aromatic benzene ring influence photocatalytic degradation activity, two chlorophenols (2,4-DCP and 2,4,6-TCP) and two chlorinated herbicides (2,4-D and 2,4,5-T) were evaluated using the optimized photocatalyst composite. It was reported that the number and positions of the chlorine substituents play vital roles in predicting the level of toxicity and degradation rate of each members of the chlorinated phenols group.[46−50] Based on the results in Figure 6, the two chlorophenols are more difficult to mineralize compared to their phenoxyacetic acid counterparts. This could be due to the difference in the oxygen functional groups (hydroxyl and acetic acid) on the aromatic ring for both classes

https://doi.org/10.1021/acs.jpcc.2c06796
J. Phys. Chem. C XXXX, XXX, XXX−XXX

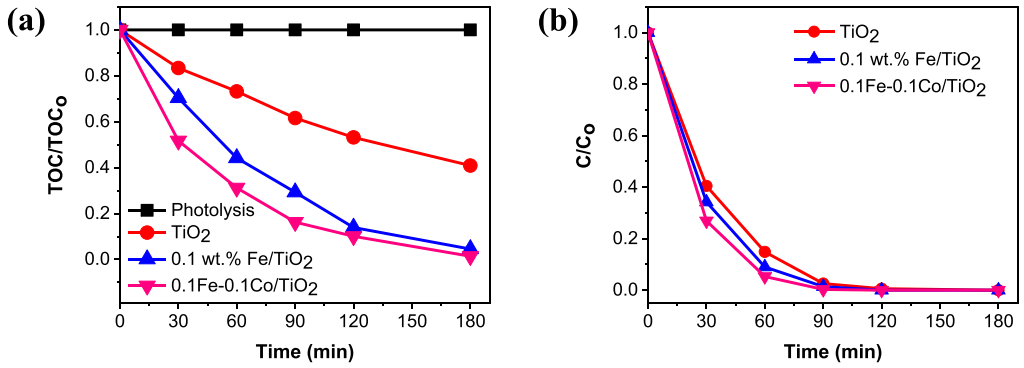

Figure 5. (a) Mineralization profiles of 2,4-D using PC50 TiO_2, FeO_x/TiO_2 and FeO_x-CoO_x/TiO_2 samples. (b) Conversion profiles of 2,4-D using PC50 TiO_2, FeO_x/TiO_2, and FeO_x-CoO_x/TiO_2 samples monitored by HPLC. Conditions: 2,4-D, 25 ppm, 200 mL, pH = 4, catalyst concentration = 0.5 g/L, λ > 320 nm.

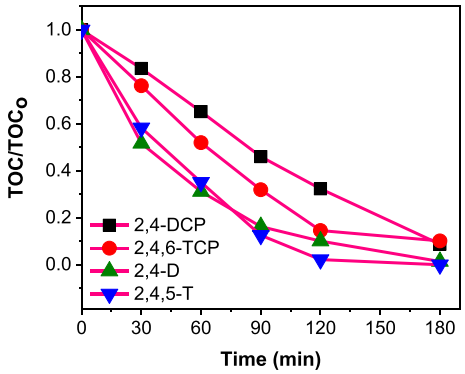

Figure 6. Mineralization profiles of selected herbicides using FeO_x-CoO_x/TiO_2 sample under similar operating conditions. Conditions: Herbicides, 25 ppm, 200 mL, pH = 4, catalyst concentration = 0.5 g/L, λ > 320 nm; 2,4-dichlorophenol (2,4-DCP), 2,4,6-trichlorophenol (2,4,6-TCP), 2,4-dichlorophenoxyacetic acid (2,4-D), 2,4,5-trichlorophenoxyacetic acid (2,4,5-T).

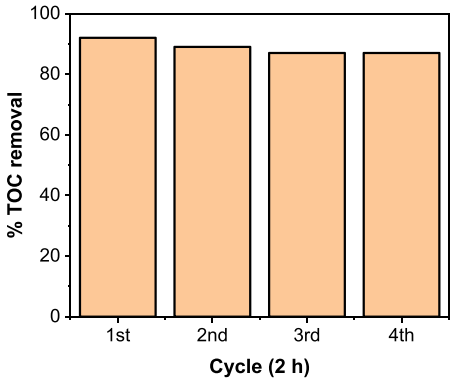

Figure 7. Recycling performance of FeO_x-CoO_x/TiO_2 for 2,4,6-TCP mineralization. Conditions: 2,4,6-TCP, 50 ppm, 200 mL, pH = 6, catalyst concentration = 0.5 g/L, λ > 260 nm.

of chlorinated herbicides, and likely the acetic acid group can be readily degraded. It is widely reported that 2,4,6-TCP degrades faster than 2,4-DCP during photocatalytic water treatment, consistent with our results in Figure 6.[48−50] However, there is no clear relationship between the degradation rate of chlorophenols and number of chlorine substituents on the aromatic ring, but the position of Cl atoms was reported to highly determine the order of initial degradation rates.[51,52] In the first 90 min, 2,4-DCP is the most difficult to mineralize, while 2,4-D and 2,4,5-T (with similar trend) are the easiest to mineralize. The temporal UV−vis absorption spectra of the four herbicides at 90 min of photocatalytic degradation on FeO_x-CoO_x/TiO_2 are shown in Figure S9a−d. The results corroborate the earlier observation with TOC removal rates as 2,4-DCP remains the most difficult to degrade, while 2,4-D and 2,4,5-T are easiest to degrade.

3.3. Catalyst Recycling and Reactive Oxygen Species Tests. The stability of the best FeO_x-CoO_x/TiO_2 composite photocatalyst was evaluated for 2,4,6-TCP mineralization under full arc light irradiation as shown in Figure 7. It can be seen that the photocatalytic activity of composite did not decrease conspicuously after four successive cycles (2 h) of 2,4,6-TCP mineralization test, indicating that the composite is fairly stable. The fair stability of FeO_x-CoO_x/TiO_2 after four successive activity cycles suggests that a small amount of CoO_x is required in the FeO_x-CoO_x/TiO_2 composite to improve its performance.

Furthermore, the loading metal content on fresh and used as-prepared samples was investigated by ICP-AES. As shown in Figure S10a−c, it can see that the actual Fe loading amount on three TiO_2-based samples is quite close to the nominal value of 0.1 wt %. However, the actual Cu and Co loading amount are far less than the designed value, possibly due to the loss during the washing procedure. The metal leaching on various photocatalysts in photocatalytic 2,4,6-TCP mineralization after recycling experiments (2 h) was then studied. It is found that approximately 64.4 wt % of Fe on FeO_x/TiO_2 was leached (Figure S10a), probably because of the severe photocorrosion. Similar phenomenon happened on FeO_x-CuO_x/TiO_2 (Figure S10b), where around 65.3 wt % of Fe and 71.2 wt % of Cu were leached respectively during the photocatalytic process. Nevertheless, the loss of Fe and Co was greatly reduced on FeO_x-CoO_x/TiO_2 (S10c). Only 51 wt % of Fe and 3.6 wt % of Co are found to be leached, indicating the good stability of the optimized FeO_x-CoO_x/TiO_2 in photocatalytic 2,4,6-TCP mineralization. Further study to improve the binding force of Fe on TiO_2 is underway.

Hydroxyl radicals ($^{\bullet}OH$) are considered the major active species during photocatalytic degradation of organic water pollutants, while the short lifetime (~10^{-9} s) and high reactivity of the hydroxyl radicals hinder its direct detection.[53,54] Fluorescence spectroscopy was used to investigate the presence of $^{\bullet}OH$ with coumarin (COU) as a probe molecule (poor fluorescent dye). The COU can react with

https://doi.org/10.1021/acs.jpcc.2c06796
J. Phys. Chem. C XXXX, XXX, XXX−XXX

•OH to give a highly fluorescent 7-hydroxycoumarin (7-HC).[54] A very low concentration (10^{-3}–10^{-4} M) of the probe molecule is often used during spectrofluorometric analysis to limit contributions from the valence band holes of TiO_2 during illumination with UV light.[55] Lower concentrations of the probe molecule usually favor hydroxylation reaction with •OH.[55,56] Figure 8 shows the fluorescence spectra of COU

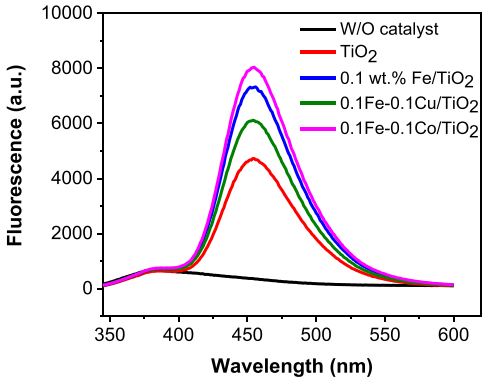

Figure 8. Fluorescence spectral changes observed during illumination of prepared TiO_2 samples in 0.001 M aqueous solution of coumarin (excitation at 332 nm). Each fluorescence spectrum was recorded after 5 min of light illumination with multichannel 300 W UV 365 nm LED.

solutions (0.001 M) containing 0.6 mg/mL of PC50 TiO_2, FeO_x/TiO_2, FeO_x–CuO_x/TiO_2, and FeO_x–CoO_x/TiO_2 under 5 min irradiation from a multichannel 300 W UV LED (365 nm). No signal was observed without a photocatalyst. The fluorescent intensities at around 455 nm follow the order: PC50 TiO_2 < FeO_x–CuO_x/TiO_2 < FeO_x/TiO_2 < FeO_x–CoO_x/TiO_2. The highest fluorescence intensity obtained from FeO_x–CoO_x/TiO_2 implies a high concentration of 7-HC, as a result of high generation rate of •OH radical, which is very beneficial for the degradation of these herbicides. This indicates that FeO_x–CoO_x/TiO_2 facilitates charge separation via hole transfer from TiO_2 as highlighted in the proposed semiconductor charge separation mechanism (Scheme 1). When the FeO_x–CoO_x/TiO_2 photocatalyst is exposed to

Scheme 1. Proposed Mechanism for Major Charge Transfer Pathways on FeO_x–CoO_x/TiO_2 for Mineralization of 2,4,6-TCP and 2,4-D

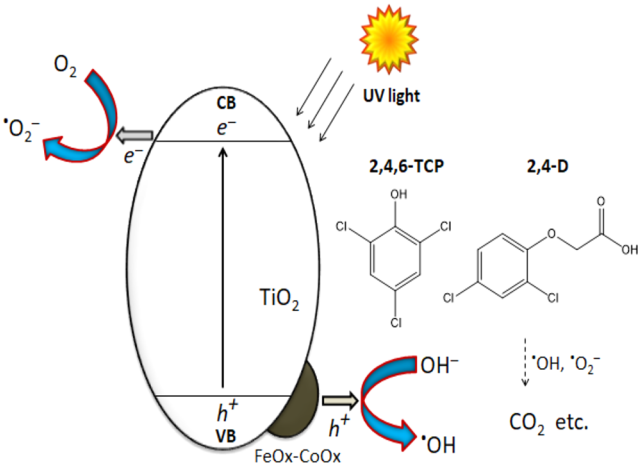

ultraviolet light, photogenerated electrons are excited from the valence band (VB) to the conduction band (CB) of TiO_2. The VB holes are transferred to the surface FeO_x/CoO_x sites and subsequently react with hydroxyl ions (OH^-) in water to produce OH radicals, which oxidize 2,4,6-TCP and other herbicides to intermediate products before their mineralization. At the same time, photoelectrons are consumed by oxygen to produce superoxides that react with the intermediates to form the final CO_2 and water.

4. CONCLUSION

In summary, a facile and robust synthesis procedure was successfully used in decorating PC50 TiO_2 nanoparticles with highly dispersed mono and dual cocatalysts (FeO_x, CuO_x, CoO_x, FeO_x–CuO_x, and FeO_x–CoO_x). The binary cocatalyst comprising FeO_x–CoO_x plays a key role for efficient decomposition of widely used four chlorinated herbicides. FeOOH (denoted as FeO_x in this article), CuO and CoO nanoparticles were determined to be the only decorating species. The highest photocatalytic 2,4,6-TCP mineralization efficiency has been achieved by the FeO_x–CoO_x/TiO_2. About 92% 2,4,6-TCP mineralization and 100% 2,4,6-TCP degradation efficiencies in 3 h are achieved over the optimized FeO_x–CoO_x/TiO_2 sample, which is about three times higher than the benchmark reference PC50 TiO_2. The optimized FeO_x–CoO_x/TiO_2 sample also exhibits 150% activity enhancement for another herbicide (2,4-D) degradation compared to TiO_2. However, the FeO_x–CoO_x/TiO_2 sample shows negligible activity for 2,4,6-TCP degradation under visible light (λ > 395 nm) irradiation. This is primarily due to the UV absorption bandgap energy of PC50 TiO_2 (3.2 eV or 390 nm), since the low concentration surface cocatalysts do not alter its bandgap based on the UV absorption spectra of the prepared photocatalysts. Under similar operating conditions, the mineralization rates with 2,4-D and 2,4,5-T are higher compared to 2,4-DCP and 2,4,6-TCP. 2,4-DCP is the most difficult to mineralize. The observation is likely due to the nature of oxygen functional groups and the relative position of Cl substituents on the aromatic ring. The enhancement in photocatalytic degradation four herbicides over the optimized FeO_x–CoO_x/TiO_2 sample is likely due to the improved change separation, hole accumulation on FeO_x–CoO_x, and enhanced hydroxyl radicals generation as FeO_x–CoO_x clusters are an excellent hole acceptor. Finally the optimized photocatalyst was proved to be rather stable for these herbicides' mineralization.

■ ASSOCIATED CONTENT

Supporting Information

The Supporting Information is available free of charge at https://pubs.acs.org/doi/10.1021/acs.jpcc.2c06796.

Figure S1, full XPS survey spectra of FeO_x–CuO_x/TiO_2 and FeO_x–CoO_x/TiO_2; Figure S2, Co 2p XPS spectra of FeO_x–CoO_x/TiO_2; Figure S3, Fe 2p XPS spectra of FeO_x–CoO_x/TiO_2; Figure S4, Ti 2p XPS spectra of TiO_2 based samples; Figure S5, mineralization profile of 2,4,6-TCP on FeO_x or/and CuO_x loaded TiO_2; Figure S6, ineralization profile of 2,4,6-TCP on FeO_x or/and CoO_x loaded TiO_2; Figure S7, TOC files with error bar on FeO_x–CoO_x/TiO_2 for 2,4,6-TCP mineralization; Figure S8, TOC files with error bar on FeO_x–CoO_x/TiO_2 for 2,4-DCP mineralization; Figure S9, temporal

https://doi.org/10.1021/acs.jpcc.2c06796
J. Phys. Chem. C XXXX, XXX, XXX–XXX

UV−vis adsorption spectra of 2.4-DCP, 2,4,6-TCP, 2,4-D, and 2,4,5-T on FeO_x−CoO_x/TiO_2 in photocatalytic degradation; and Figure S10, metal loading amount on fresh and used TiO_2-based samples detected by ICP-AES. (PDF)

AUTHOR INFORMATION

Corresponding Author

Junwang Tang − *Department of Chemical Engineering, University College London, London WC1E 7JE, U.K.*; orcid.org/0000-0002-2323-5510; Email: junwang.tang@ucl.ac.uk

Authors

Ayoola Shoneye − *Department of Chemical Engineering, University College London, London WC1E 7JE, U.K.*

Haimiao Jiao − *Department of Chemical Engineering, University College London, London WC1E 7JE, U.K.*

Complete contact information is available at: https://pubs.acs.org/10.1021/acs.jpcc.2c06796

Notes

The authors declare no competing financial interest.

ACKNOWLEDGMENTS

A. Shoneye acknowledges studentship from the Federal Scholarship Board (FSB), Nigeria. H. Jiao and J. Tang acknowledge funding from EPSRC (EP/S018204/2), Royal Society International Exchanges (IEC\NSFC\170342), and the Leverhulme Trust (RPG-2017-122).

REFERENCES

(1) Hejazi, S.; Yadolahi, J.; Shahverdi, M.; Malakootikhah, J. Identifying Nanotechnology-Based Entrepreneurial Opportunities in Line Withwater-Related Problems. *Middle East J. Sci. Res.* **2011**, *8*, 337−348.

(2) Okoli, C. P.; Diagboya, P. N.; Anigbogu, I. O.; Olu-Owolabi, B. I.; Adebowale, K. O. Competitive Biosorption of Pb(Ii) and Cd(Ii) Ions from Aqueous Solutions Using Chemically Modified Moss Biomass (Barbula Lambarenensis). *Environ. Earth Sci.* **2017**, *76*, 33−33.

(3) Gómez-Pastora, J.; Dominguez, S.; Bringas, E.; Rivero, M. J.; Ortiz, I.; Dionysiou, D. D. Review and Perspectives on the Use of Magnetic Nanophotocatalysts (Mnpcs) in Water Treatment. *Chem. Eng. J.* **2017**, *310*, 407−427.

(4) Olaniran, A. O.; Igbinosa, E. O. Chlorophenols and Other Related Derivatives of Environmental Concern: Properties, Distribution and Microbial Degradation Processes. *Chemosphere* **2011**, *83*, 1297−306.

(5) Navarro, S.; Fenoll, J.; Vela, N.; Ruiz, E.; Navarro, G. Photocatalytic Degradation of Eight Pesticides in Leaching Water by Use of ZnO under Natural Sunlight. *J. Hazard. Mater.* **2009**, *172*, 1303−10.

(6) Keith, L.; Telliard, W. Es&T Special Report: Priority Pollutants: I-a Perspective View. *Environ. Sci. Technol.* **1979**, *13*, 416−423.

(7) Rengaraj, S.; Li, X. Enhanced Photocatalytic Activity of TiO_2 by Doping with Ag for Degradation of 2, 4, 6-Trichlorophenol in Aqueous Suspension. *J. Mol. Catal. A: Chem.* **2006**, *243*, 60−67.

(8) Sharma, S.; Mukhopadhyay, M.; Murthy, Z. V. P. Treatment of Chlorophenols from Wastewaters by Advanced Oxidation Processes. *Sep. Purif. Rev.* **2013**, *42*, 263−295.

(9) Choi, K.-H.; Min, J.; Park, S.-Y.; Park, B. J.; Jung, J.-S. Enhanced Photocatalytic Degradation of Tri-Chlorophenol by Fe_3O_4@ TiO_2@ Au Photocatalyst under Visible-Light. *Ceram. Int.* **2019**, *45*, 9477−9482.

(10) Gusain, R.; Gupta, K.; Joshi, P.; Khatri, O. P. Adsorptive Removal and Photocatalytic Degradation of Organic Pollutants Using Metal Oxides and Their Composites: A Comprehensive Review. *Adv. Colloid Interface Sci.* **2019**, *272*, 102009.

(11) Khaki, M. R. D.; Shafeeyan, M. S.; Raman, A. A. A.; Daud, W. M. A. W. Application of Doped Photocatalysts for Organic Pollutant Degradation - a Review. *J. Environ. Manage.* **2017**, *198*, 78−94.

(12) Shoneye, A.; Tang, J. Highly Dispersed FeOOH to Enhance Photocatalytic Activity of TiO_2 for Complete Mineralisation of Herbicides. *Appl. Surf. Sci.* **2020**, *511*, 145479.

(13) Yuliati, L.; Roslan, N. A.; Siah, W. R.; Lintang, H. O. Cobalt Oxide-Modified Titanium Dioxide Nanoparticle Photocatalyst for Degradation of 2, 4-Dichlorophenoxyacetic Acid. *Indones. J. Chem.* **2017**, *17*, 284−290.

(14) An, X.; Liu, H.; Qu, J.; Moniz, S. J. A.; Tang, J. Photocatalytic Mineralisation of Herbicide 2,4,5-Trichlorophenoxyacetic Acid: Enhanced Performance by Triple Junction Cu−TiO_2−Cu_2O and the Underlying Reaction Mechanism. *New J. Chem.* **2015**, *39*, 314−320.

(15) Ahadi, S.; Moalej, N. S.; Sheibani, S. Characteristics and Photocatalytic Behavior of Fe and Cu Doped TiO_2 Prepared by Combined Sol-Gel and Mechanical Alloying. *Solid State Sci.* **2019**, *96*, 105975.

(16) Castañeda-Juárez, M.; Martínez-Miranda, V.; Almazán-Sánchez, P. T.; Linares-Hernández, I.; Santoyo-Tepole, F.; Vázquez-Mejía, G. Synthesis of TiO_2 Catalysts Doped with Cu, Fe, and Fe/Cu Supported on Clinoptilolite Zeolite by an Electrochemical-Thermal Method for the Degradation of Diclofenac by Heterogeneous Photocatalysis. *J. Photochem. Photobiol., A* **2019**, *380*, 111834.

(17) Apiwong-ngarm, K.; Pongwan, P.; Inceesungvorn, B.; Phanichphant, S.; Wetchakun, K.; Wetchakun, N. Photocatalytic Activities of Fe−Cu/TiO_2 on the Mineralization of Oxalic Acid and Formic Acid under Visible Light Irradiation. *Powder Technol.* **2014**, *266*, 447−455.

(18) Bhardwaj, S.; Pal, B. Photodeposition of Ag and Cu Binary Co-Catalyst onto TiO_2 for Improved Optical and Photocatalytic Degradation Properties. *Adv. Powder Technol.* **2018**, *29*, 2119−2128.

(19) Guerrero-Araque, D.; Acevedo-Peña, P.; Ramírez-Ortega, D.; Lartundo-Rojas, L.; Gómez, R. SnO_2−TiO_2 Structures and the Effect of CuO, CoO Metal Oxide on Photocatalytic Hydrogen Production. *J. Chem. Technol. Biotechnol.* **2017**, *92*, 1531−1539.

(20) Neubert, S.; Mitoraj, D.; Shevlin, S. A.; Pulisova, P.; Heimann, M.; Du, Y.; Goh, G. K.; Pacia, M.; Kruczała, K.; Turner, S.; et al. Highly Efficient Rutile TiO_2 Photocatalysts with Single Cu(Ii) and Fe(Iii) Surface Catalytic Sites. *J. Mater. Chem. A* **2016**, *4*, 3127−3138.

(21) Liu, Y.; Sun, Z.; Hu, Y. H. Bimetallic Cocatalysts for Photocatalytic Hydrogen Production from Water. *Chem. Eng. J.* **2021**, *409*, 128250.

(22) Neubert, S.; Pulisova, P.; Wiktor, C.; Weide, P.; Mei, B.; Guschin, D. A.; Fischer, R. A.; Muhler, M.; Beranek, R. Enhanced Photocatalytic Degradation Rates at Rutile TiO_2 Photocatalysts Modified with Redox Co-Catalysts. *Catal. Today* **2014**, *230*, 97−103.

(23) Rao, G.; Zhao, H.; Chen, J.; Deng, W.; Jung, B.; Abdel-Wahab, A.; Batchelor, B.; Li, Y. FeOOH and Fe_2O_3 Co-Grafted TiO_2 Photocatalysts for Bisphenol a Degradation in Water. *Catal. Commun.* **2017**, *97*, 125−129.

(24) Wu, J.; Li, C.; Zhao, X.; Wu, Q.; Qi, X.; Chen, X.; Hu, T.; Cao, Y. Photocatalytic Oxidation of Gas-Phase Hg0 by CuO/TiO_2. *Appl. Catal., B* **2015**, *176*, 559−569.

(25) Moniz, S. J.; Tang, J. Charge Transfer and Photocatalytic Activity in CuO/TiO_2 Nanoparticle Heterojunctions Synthesised through a Rapid, One-Pot, Microwave Solvothermal Route. *ChemCatChem.* **2015**, *7*, 1659−1667.

(26) Zhou, G.; Dong, Y.; He, D. Bimetallic Ru−M/TiO_2 (M= Fe, Ni, Cu, Co) Nanocomposite Catalysts Facribated by Galvanic Replacement: Structural Elucidation and Catalytic Behavior in Benzene Selective Hydrogenation. *Appl. Surf. Sci.* **2018**, *456*, 1004−1013.

(27) Qiu, X.; Miyauchi, M.; Sunada, K.; Minoshima, M.; Liu, M.; Lu, Y.; Li, D.; Shimodaira, Y.; Hosogi, Y.; Kuroda, Y.; et al. Hybrid Cu_xO/TiO_2 Nanocomposites as Risk-Reduction Materials in Indoor Environments. *ACS Nano* **2012**, *6*, 1609−1618.
(28) Zhu, L.; Zeng, Y.; Zhang, S.; Deng, J.; Zhong, Q. Effects of Synthesis Methods on Catalytic Activities of CoO_x−TiO_2 for Low-Temperature NH_3-SCR of NO. *J. Environ. Sci.* **2017**, *54*, 277−287.
(29) Petitto, S.; Langell, M. Surface Composition and Structure of Co_3O_4 (110) and the Effect of Impurity Segregation. *J. Vac. Sci. Technol., A* **2004**, *22*, 1690−1696.
(30) Shen, Z.-X.; Allen, J.; Lindberg, P.; Dessau, D.; Wells, B.; Borg, A.; Ellis, W.; Kang, J.; Oh, S.-J.; Lindau, I.; et al. Photoemission Study of CoO. *Phys. Rev. B* **1990**, *42*, 1817.
(31) Moniz, S.; Shevlin, S.; Martin, D.; Guo, Z. X.; Tang, J. Visible-Light Driven Heterojunction Photocatalysts for Water Splitting− a Critical Review. *Energy Environ. Sci.* **2015**, *8*, 731−759.
(32) Xie, J.; Jin, R.; Li, A.; Bi, Y.; Ruan, Q.; Deng, Y.; Zhang, Y.; Yao, S.; Sankar, G.; Ma, D.; et al. Highly Selective Oxidation of Methane to Methanol at Ambient Conditions by Titanium Dioxide-Supported Iron Species. *Nat. Catal.* **2018**, *1*, 889−896.
(33) McIntyre, N.; Zetaruk, D. X-Ray Photoelectron Spectroscopic Studies of Iron Oxides. *Anal. Chem.* **1977**, *49*, 1521−1529.
(34) Yamashita, T.; Hayes, P. Analysis of XPS Spectra of Fe^{2+} and Fe^{3+} Ions in Oxide Materials. *Appl. Surf. Sci.* **2008**, *254*, 2441−2449.
(35) Ding, Y.; Sun, W.; Cao, L.; Yang, J. A Spontaneous Catalytic Membrane Reactor to Dechlorinate 2,4,6-TCP as an Organic Pollutant in Wastewater and to Reclaim Electricity Simultaneously. *Chem. Eng. J.* **2016**, *285*, 573−580.
(36) Mylonas, A.; Papaconstantinou, E. Photocatalytic Degradation of Chlorophenols to CO_2 and HCl with Polyoxotungstates in Aqueous Solution. *J. Mol. Catal.* **1994**, *92*, 261−267.
(37) Burrows, H. D.; Ernestova, L. S.; Kemp, T. J.; Skurlatov, Y. I.; Purmal, A. P.; Yermakov, A. N. Kinetics and Mechanism of Photodegradation of Chlorophenols. *Prog. React. Kinet.* **1998**, *23*, 145−207.
(38) Legrini, O.; Oliveros, E.; Braun, A. Photochemical Processes for Water Treatment. *Chem. Rev.* **1993**, *93*, 671−698.
(39) Fu, F.; Shen, H.; Sun, X.; Xue, W.; Shoneye, A.; Ma, J.; Luo, L.; Wang, D.; Wang, J.; Tang, J. Synergistic Effect of Surface Oxygen Vacancies and Interfacial Charge Transfer on Fe (III)/Bi_2MoO_6 for Efficient Photocatalysis. *Appl. Catal., B* **2019**, *247*, 150−162.
(40) Kim, T. W.; Choi, K.-S. Nanoporous $BiVO_4$ Photoanodes with Dual-Layer Oxygen Evolution Catalysts for Solar Water Splitting. *Science* **2014**, *343*, 990−994.
(41) Oehler, F.; Naumann, R.; Köferstein, R.; Hesse, D.; Ebbinghaus, S. G. Photocatalytic Activity of $CaTaO_2N$ Nanocrystals Obtained from a Hydrothermally Synthesized Oxide Precursor. *Mater. Res. Bull.* **2016**, *73*, 276−283.
(42) Oehler, F.; Ebbinghaus, S. G. Photocatalytic Properties of CoO_x-Loaded Nano-Crystalline Perovskite Oxynitrides ABO_2N (A= Ca, Sr, Ba, La; B= Nb, Ta). *Solid State Sci.* **2016**, *54*, 43−48.
(43) Zhang, F.; Yamakata, A.; Maeda, K.; Moriya, Y.; Takata, T.; Kubota, J.; Teshima, K.; Oishi, S.; Domen, K. Cobalt-Modified Porous Single-Crystalline $LaTiO_2N$ for Highly Efficient Water Oxidation under Visible Light. *J. Am. Chem. Soc.* **2012**, *134*, 8348−8351.
(44) Barroso, M.; Cowan, A. J.; Pendlebury, S. R.; Grätzel, M.; Klug, D. R.; Durrant, J. R. The Role of Cobalt Phosphate in Enhancing the Photocatalytic Activity of A-Fe_2O_3 toward Water Oxidation. *J. Am. Chem. Soc.* **2011**, *133*, 14868−14871.
(45) Kamata, K.; Maeda, K.; Lu, D.; Kako, Y.; Domen, K. Synthesis and Photocatalytic Activity of Gallium−Zinc−Indium Mixed Oxynitride for Hydrogen and Oxygen Evolution under Visible Light. *Chem. Phys. Lett.* **2009**, *470*, 90−94.
(46) Czaplicka, M. Sources and Transformations of Chlorophenols in the Natural Environment. *Sci. Total Environ.* **2004**, *322*, 21−39.
(47) Pandiyan, T.; Martınez Rivas, O.; Orozco Martınez, J.; Burillo Amezcua, G.; Martınez-Carrillo, M.A. Comparison of Methods for the Photochemical Degradation of Chlorophenols. *J. Photochem. Photobiol., A* **2002**, *146*, 149−155.
(48) Ma, Y.; Zhang, Y.; Zhu, X.; Lu, N.; Li, C.; Yuan, X.; Qu, J. Photocatalytic Degradation and Rate Constant Prediction of Chlorophenols and Bisphenols by $H_3PW_{12}O_{40}$/GR/TiO_2 Composite Membrane. *Environ. Res.* **2020**, *188*, 109786.
(49) Zhen, Y.; Zhang, Q.; Zhang, X.; Zhang, G.; Chen, X.; Zhao, C. A Novel Tubular up-Flow Magnetic Film Photocatalytic System Optimized by Main Factors Control for Efficient Removal of Chlorophenols Wastewater. *J. Hazard. Mater.* **2020**, *398*, 122963.
(50) Yang, J.; Cui, S.; Qiao, J.-q.; Lian, H.-z. The Photocatalytic Dehalogenation of Chlorophenols and Bromophenols by Cobalt Doped Nano TiO_2. *J. Mol. Catal. A: Chem.* **2014**, *395*, 42−51.
(51) Antonaraki, S.; Androulaki, E.; Dimotikali, D.; Hiskia, A.; Papaconstantinou, E. Photolytic Degradation of All Chlorophenols with Polyoxometallates and H_2O_2. *J. Photochem. Photobiol., A* **2002**, *148*, 191−197.
(52) Kochany, J.; Bolton, J. R. Mechanism of Photodegradation of Aqueous Organic Pollutants. 1. Epr Spin-Trapping Technique for the Determination of Hydroxyl Radical Rate Constants in the Photooxidation of Chlorophenols Following the Photolysis of Hydrogen Peroxide. *J. Phys. Chem.* **1991**, *95*, 5116−5120.
(53) Yang, J.; Chen, H.; Gao, J.; Yan, T.; Zhou, F.; Cui, S.; Bi, W. Synthesis of Fe_3O_4/g-C_3N_4 Nanocomposites and Their Application in the Photodegradation of 2, 4, 6-Trichlorophenol under Visible Light. *Mater. Lett.* **2016**, *164*, 183−189.
(54) Xiang, Q.; Yu, J.; Wong, P. K. Quantitative Characterization of Hydroxyl Radicals Produced by Various Photocatalysts. *J. Colloid Interface Sci.* **2011**, *357*, 163−167.
(55) Ishibashi, K.-i.; Fujishima, A.; Watanabe, T.; Hashimoto, K. Detection of Active Oxidative Species in TiO_2 Photocatalysis Using the Fluorescence Technique. *Electrochem. Commun.* **2000**, *2*, 207−210.
(56) Goldstein, S.; Czapski, G.; Rabani, J. Oxidation of Phenol by Radiolytically Generated. Bul. OH and Chemically Generated SO_4. Bul.-. A Distinction Between. Bul. OH Transfer and Hole Oxidation in the Photolysis of TiO_2 Colloid Solution. *J. Phys. Chem.* **1994**, *98*, 6586−6591.

https://doi.org/10.1021/acs.jpcc.2c06796
J. Phys. Chem. C XXXX, XXX, XXX−XXX